J. Eng. Technol. Sci., Vol. 53, No. 3, 2021, 210301

Seismic Behavior of Concrete-Filled Steel Tube (CFST) Column and Reinforced Concrete (RC) Beam Connections under Reversed Cyclic Loading

Ahmed Najm Abdullah[1*], Bambang Budiono[2], Herlien Dwiarti Setio[2] & Erwin Lim[2]

[1]Post-Graduate Program of Civil Engineering Department,
Faculty of Civil and Environmental Engineering, Institut Teknologi Bandung,
Jalan Ganesha No. 10, Bandung 40132, Indonesia
[2]Structure Research Group, Civil Engineering Department,
Faculty of Civil and Environmental Engineering, Institut Teknologi Bandung,
Jalan Ganesha No. 10, Bandung 40132, Indonesia
*E-mail: inf.ahmednajm@gmail.com

Highlights:

- The proposed CFST column and RC beam subassemblies were provided with a continuous steel tube. This design conforms to strong column/weak beam criteria and sufficient joint shear strength.
- The test results show that continuous steel tube provides sufficient joint confinement, prevents severe cracks, and controls shear deformation.
- Sliding shear was observed during the test, however, the performance can be improved by providing sufficient sliding shear resistance along the beam.
- The hysteretic behavior showed satisfactory seismic performance.
- A correctly modeled finite element can properly capture the overall hysteretic behavior of the proposed subassemblies.
- The new connections indicate potential application in precast systems.

Abstract. Previous studies on the connection between concrete-filled steel tube (CFST) columns and reinforced concrete (RC) beams have shown a loss of joint confinement because the steel tube was completely or partially cut in the joint area. This research presents a new connection system that provides joint confinement through a continuous steel tube. Potential sliding shear at the smooth interface between the columns and beams in the joint face is mitigated using two mechanisms: (i) shear connectors and (ii) longitudinal web beam reinforcement. This study tested two CFST column and RC beam joints to 4.5% drift ratio under combined compression axial load and lateral cyclic load. The experimental results revealed no cracks at the joint zone and the specimens satisfied the ACI 374.1-05 criteria, despite minor sliding at the beam-column interface. The finite element (FE) model showed good agreement with the experimental results.

Keywords: *concrete-filled steel tube (CFST); continuous steel tube; finite-element model; new connections; RC beam; seismic performance; sliding shear.*

Received June 30th, 2020, 1st Revision September 30th, 2020, 2nd Revision October 12th, 2020, Accepted for publication November 19th, 2020.

DOI: 10.5614/j.eng.technol.sci.2021.53.3.1

1 Introduction

In recent decades, concrete filled steel tube (CFST) columns have been utilized often in high-rise buildings because of their specific mechanical and seismic behaviors such as strength, stiffness, good ductility and convenience for construction. The concrete core of CFST columns increases their stability while the steel tube provides full confinement of the concrete core and serves as the formwork during the construction process. Therefore, CFST columns are utilized as the primary structural elements to resist the vertical and lateral loads in high-rise buildings [1]. A major challenge in constructing CFST structures is the joint between the columns and beams. Several studies [2-6] have investigated the behavior of joints between CFST columns and RC beams. In those studies, the steel tube was cut completely or partially in the joint zone. In addition, the longitudinal bars in the RC beams were continuous through the joint. In order to compensate for the loss of joint confinement, an additional RC ring beam was used (Figure 1(a)). Experiments showed that these connections provide good strength, stiffness, and energy dissipation. However, the construction of a ring beam has several disadvantages, such as the complexity of the reinforcement details within the ring beam, the difficulty of installing curtain walls, which may affect the architectural look, and the difficulty of welding on the construction site.

This research proposes new joint systems to eliminate the aforementioned disadvantages. In the proposed joints, the joint confinement is preserved by providing a continuous steel column tube through the joint zone. In addition, holes in the steel tube of the column (Figure 1(b)) allow for the installment of continuous longitudinal beam reinforcements. These types of connections are easy to construct, architecturally desirable, and show potential use as a precast system.

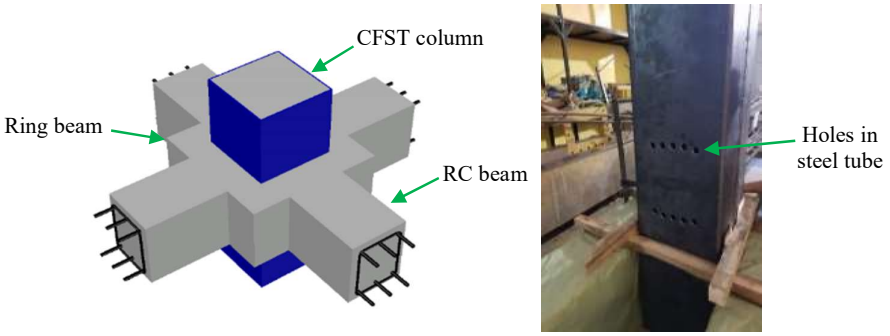

Figure 1 Two kinds of joint systems: (a) CFST column to RC beam connection with ring beam, and (b) proposed connection with continuous steel tube.

Potential sliding shear failure because of the continuous steel tube is reduced by using shear connectors or longitudinal web beam reinforcement. As part of this study, two specimens were designed and fabricated, which differed in how they prevent the occurrence of sliding shear. The specimens were tested under combined axial compression and lateral cyclic loading to examine their strength, stiffness, and energy dissipation. The results demonstrated that the proposed connections have favorable seismic performance satisfying the ACI 374.1-05 [7] criteria despite the occurrence of sliding shear failure causing minor pinching in the hysteretic curves. A finite-element model was built using a commercial package and showed good agreement with the experimental results.

2 Experimental Program

2.1 Specimen Details

Two CFST column and RC beam connection specimens of the same dimensions were cast in the laboratory. They reflect a plane frame structure of beam-column joints taken from the interior connections. The specimens were designed to achieve satisfactory seismic performance by following strong column/weak beam and sufficient joint shear strength criteria, so that failure is expected to occur at the beam end. The beam length was 1500 mm on each side of the joint and the column height was 2100 mm, as shown in Figures 2 and 3. The columns were made of a 6-mm thick hollow square steel tube and filled with normal-strength concrete. Meanwhile, the cross-sectional dimension of the beams was 260 mm x 320 mm. In addition, the cross-sectional dimension of the columns was 340 mm x 340 mm. The two connections differ in the way they resist potential sliding shear at the beam-column interface.

In specimen CFST-6SC, five D16s were used as longitudinal tensile and compression reinforcement bars for the beams. Potential sliding shear was prevented by adding a shear connector at the beam-column interface, as shown in Figure 2. This shear connector was constructed using 6-mm thick steel to encase the beam over a length of 65 mm measured from the column face (Figure 2), which was welded to the column steel tube.

The second specimen (CFST-6RB) was designed to resist potential sliding shear through longitudinal web reinforcement of the beam. Five D16 rebars were provided as top and bottom longitudinal beam reinforcement, and three D13 rebars were distributed to resist potential sliding shear on each side (Figure 3). Due to this detailing, the flexural strength of the beams in the first and second specimen differed slightly. Nevertheless, they both satisfied the design criteria and were expected to exhibit equally satisfactory seismic behavior. The details of the designs are presented in Sections 2.3 and 2.4 below.

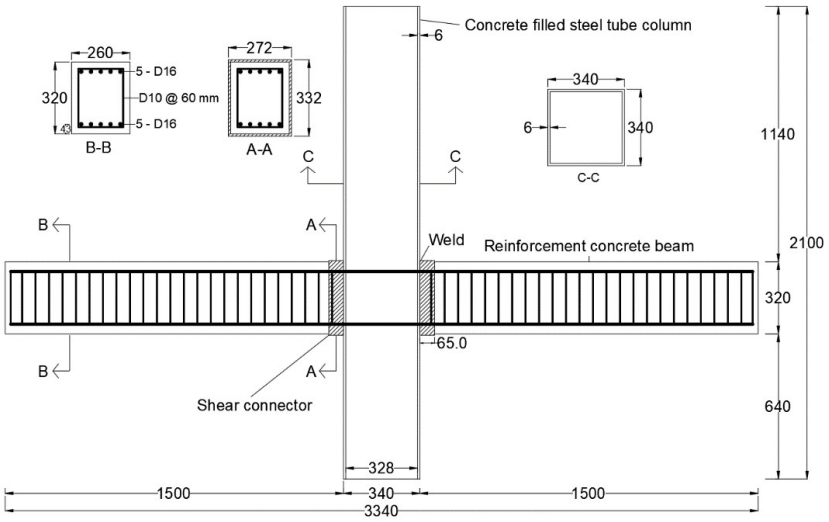

Figure 2 Details of specimen CFST-6SC in millimeters.

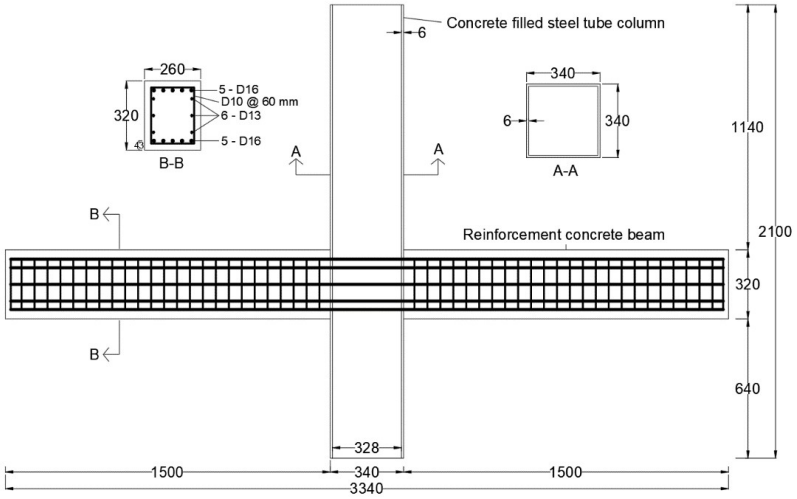

Figure 3 Details of specimen CFST-6RB in millimeters.

2.2 Materials

The specimens were cast with the same batch of concrete. Six standard concrete cylinders were prepared and cured under the same condition as the specimens. The concrete test was done according to ASTM C39/C39M [8] and the average

concrete strength f'_c of the specimens was 36.74 MPa. A tensile test of the steel plate and the reinforcement bars was conducted according to ASTM A370 [9] to define the mechanical properties of steel, as shown in Table 1.

Table 1 Measured mechanical properties of reinforcement bars and steel plate.

Material	Yield strength, (MPa)	Yield strain	Tensile strength, (MPa)	Tensile strain	Modulus of elasticity, (MPa)
Deformed steel bar (16 mm)	437.40	0.00199	648.56	0.125	219798.99
Deformed steel bar (13 mm)	429.33	0.00197	658.48	0.120	217934.01
Deformed steel bar (10 mm)	472.46	0.00245	691.22	0.110	192840.81
Steel plate – thick (6 mm)	252.47	0.00138	324.38	0.209	182949.27

2.3 Design of Specimens

In general, the specimens were designed to fail in beam flexure. Therefore, the beam, column and joint elements were designed to satisfy strong column-weak beam, sufficient joint shear strength, and sliding shear strength criteria. The beam flexural strength (M_b) was determined using a strain compatibility method according to ACI 318 [10]. Meanwhile, column flexural strength (M_c) was obtained using a simplified full plastic stress distribution according to AISC 360-16 [11]. The exalted compression axial load was $0.1 f'_c A_g$ on top of the column, where f'_c is the average standard cylinder compressive strength of concrete and A_g is the gross area of the column. The material properties obtained from the test were used in this calculation. Table 2 presents the column to beam flexural strength ratios. The beams of the CFST-6RB specimen have higher flexural strength because of the additional web beam reinforcement, which was provided to resist the sliding shear. The joint shear strength was determined according to the AIJ standard [12] using Eq. (1):

$$V_n = \tau_{cu} A_c + \tau_{su} \frac{A_s}{2} \tag{1}$$

where, τ_{cu} and τ_{su} are the ultimate shear stresses of the concrete and steel tubes, respectively, as shown in Eqs. (2), (3), and (4):

$$\tau_{cu} = J \times min\,(0.12 f'_c,\ 1.8 + 0.036 f'_c) \tag{2}$$

$$J = \frac{2.5 L_w}{d} \tag{3}$$

$$\tau_{su} = \frac{1.2}{\sqrt{3}} f_y \tag{4}$$

In the above equations, f_y is the yield stress of the steel tube, A_c is the area of concrete portion, A_s is the area of the steel tube, L_w is the width of the column, and d is the depth of the beam. The ratio of joint shear strength to joint shear force (V_n/V_{jh}) were 1.54 and 1.34 for specimens CFST-6SC and CFST-6RB, respectively, as shown in Table 2.

Table 2 Summary of specimen information.

Specimen	Axial load level, kN	M_c (kN.m)	M_b (kN.m)	$(\sum M_c/\sum M_b)$ ratio	(V_n/V_{jh}) ratio
CFST-6SC	424.71	330.00	107.06	3.00	1.54
CFST-6RB	424.71	330.00	132.65	2.50	1.34

2.4 Design of Sliding Shear

Sliding shear may occur because of the smooth interface between the beam and column caused by the continuous steel tube. The design of sliding shear resistance for the CFST-6SC specimen concerns the interfaces between the columns and the beams. Therefore, a shear connector was used in this specimen. The critical section was moved from the interface to the end of the shear connector, as shown in Figure 4(a), because a constant shear force acts along the beam.

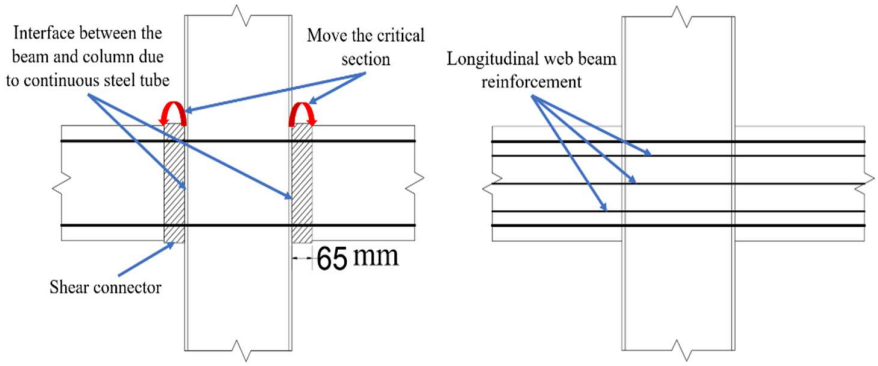

Figure 4 Mechanism of resisting the sliding shear: (a) movement of the critical section in the CFST-6SC specimen, (b) longitudinal web reinforcement in the CFST-6RB specimen.

The CFST-6RB specimen was designed to resist sliding shear by providing a continuous web beam reinforcement, as shown in Figure 4(b). The amount of web beam reinforcement was determined according to $V_{sn} = \mu A_v f_s$ [10], where μ is the coefficient of friction, which equals 1; A_v is the area of the longitudinal web reinforcement crossing the sliding shear plane; and f_s is the residual tensile stress

of the web reinforcement after deducting the contribution of its flexural strength. The ratio of sliding shear strength to sliding shear force was 2.72 and 1.62 for specimens CFST-6SC and CFST-6RB, respectively.

2.5 Test Setup, Loading Protocol, and Instrumentation

The test setup of the specimens is shown in Figure 5. The columns and beams were connected at the ends with a joint support to represent inflection points in the mid-span of the element. Both ends of the beams and columns were restrained laterally to avoid movement outside the loading direction during the test. The beam's end was connected to a roller support and the column base was pinned to a strong floor. An alternating lateral cyclic load was applied to the column top through a hydraulic actuator with a capacity of 1000 kN supported by a strong steel frame. A constant axial compression load was applied to the column top by a hydraulic jack with a capacity of 1000 kN. This was mounted on a strong plate (thickness 65 mm) and pressed four steel bars with a diameter of 32 mm. Then, the four steel bars pressed on the columns to provide the axial load.

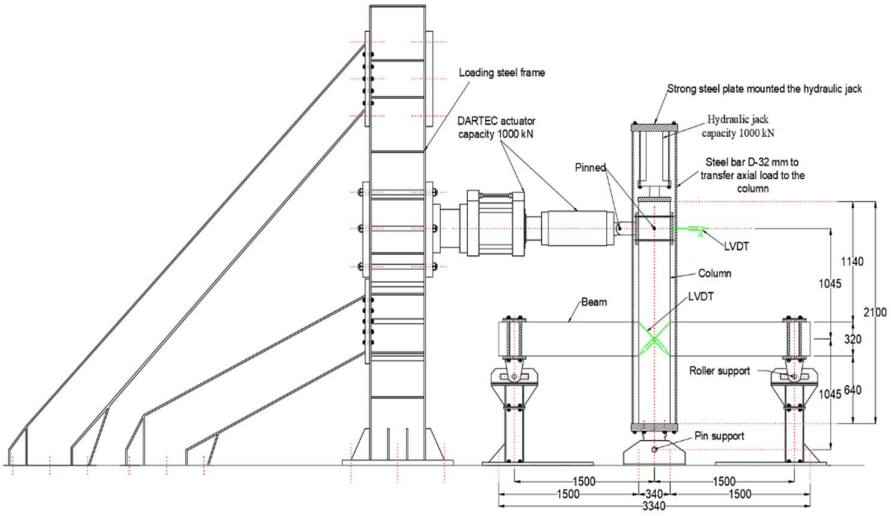

Figure 5 Test setup.

The lateral load was applied to the specimens in a displacement-controlled mode according to ACI 374.1.05 [7], as shown in Figure 6. The lateral load had 12 different drift levels, which increased from 0.2% to 4.5%. Linear variable displacement transducers (LVDTs) were installed at the connection and at the top of the column to observe the behavior in those locations (see Figure 5).

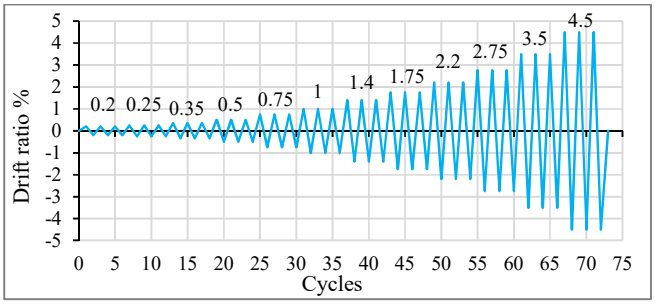

Figure 6 Lateral loading history applied on the specimens.

3 Experimental Results and Discussion

3.1 Hysteretic Curves

Figure 7 shows the hysteresis curves with important events recorded during the test, such as first bending crack, first yield of the longitudinal bar, and spalling of the concrete cover of the specimens under cyclic loading. The hysteretic curves were initially elastic and close to linear. With increasing drift ratio, the specimens entered the inelastic response and a minor pinch effect was observed, however, the specimens maintained their strength until the end of the test.

The following observations were recorded from the experimental data: (1) the first bending crack occurred before the yield strength of the longitudinal reinforcement of the beam; (2) the specimens showed maximum lateral resistance before spalling of the concrete cover occurred; (3) no core crushing occurred after the yielding of the longitudinal bars even with high yield stress (this mode of failure is desirable); and (4) spalling of the concrete cover was observed in the specimens at a drift ratio of 4.5%. The lateral resistance of the specimens as governed by the moment capacity of the beam and the ultimate lateral resistance differed slightly between the two specimens. This was due to the additional longitudinal web beam reinforcement of the beam of specimen CFST-6RB.

Figure 8 shows the variation of the lateral load versus joint shear distortion. The joint shear distortion values were relatively small as the specimens satisfied the requirement of a strong joint/weak beam. Therefore, the joint of this specimen was still within the elastic stage. However, the longitudinal web reinforcements in CFST-6RB increased the joint shear distortions due to the increased ratio of the beam to column flexural capacity in this specimen.

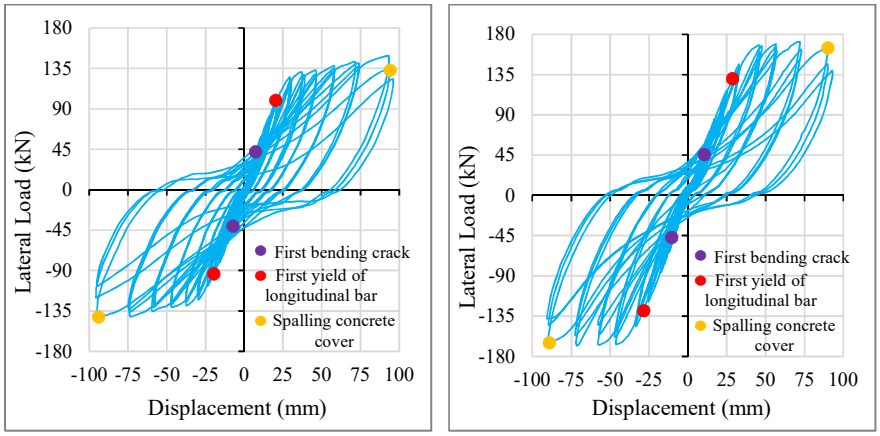

Figure 7 Experimental hysteretic curves: (a) CFST-6SC and (b) CFST-6RB.

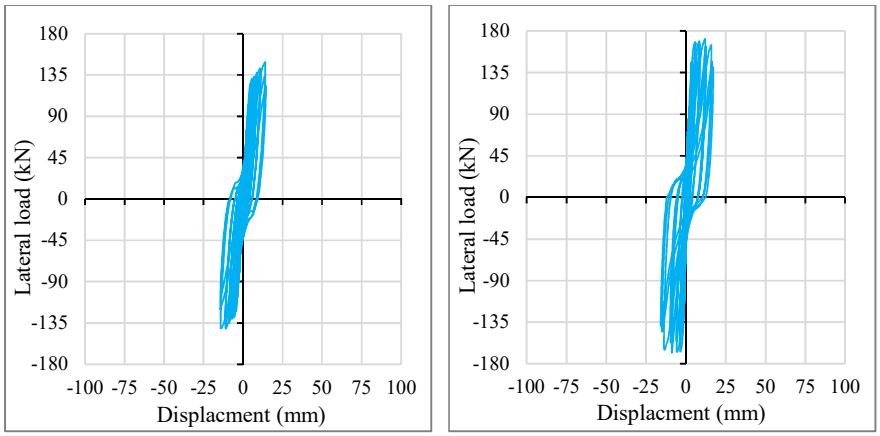

Figure 8 Lateral load versus joints shear distortion curves: (a) CFST-6SC and (b) CFST-6RB.

3.2 Failure Mode

Failure mode was characterized by beam flexural failure, followed by sliding shear failure. This was observed in specimen CFST-6SC at the beams outside the shear connector, as can be seen in Figure 9(a). At this location, the beam cover spalled and sliding shear occurred. In specimen CFST-6RB, failure was observed at the beam outside the joint as in Figure 9(b). The concrete of the beam spalled

near the joint zone and a vertical gap emerged between the column face and the RC beam because the beam longitudinal reinforcement slipped.

In both specimens, no damage occurred in the concrete core of the beams. The flexure-sliding shear failure under cyclic load could not be prevented by merely providing the web reinforcement that was tested in the present study. Therefore, the energy dissipation capacity and overall hysteretic behavior can be affected. Nevertheless, the seismic behavior of the specimens satisfied the ACI 374.1-05 criteria [7].

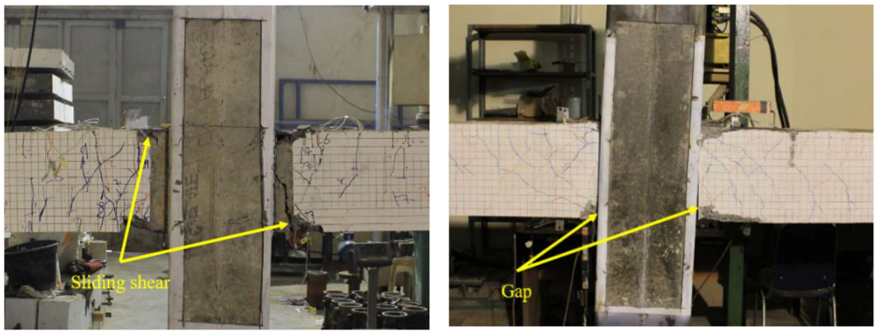

(a) (b)

Figure 9 Final crack pattern (failure mode): (a) CFST-6SC and (b) CFST-6RB.

The relationship between the lateral load versus strain at gauging points 1 and 2 (as in Figure 10) is presented in Figures 11 and 12. This study found that the strain value did not exceed the yield strain at maximum lateral resistance. After each test, the column's steel tube was removed to investigate cracks in the concrete (Figure 9). No cracking occurred in the joint zone and the column due to the confinement of the concrete core provided by the steel tube. Also, no yielding was observed in the column's steel tube. Thus, the joints and columns of both specimens remained in the elastic stage throughout the entire test.

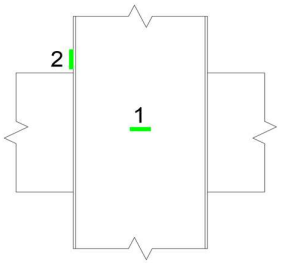

Figure 10 Arrangement of strain gauges on the steel tube column.

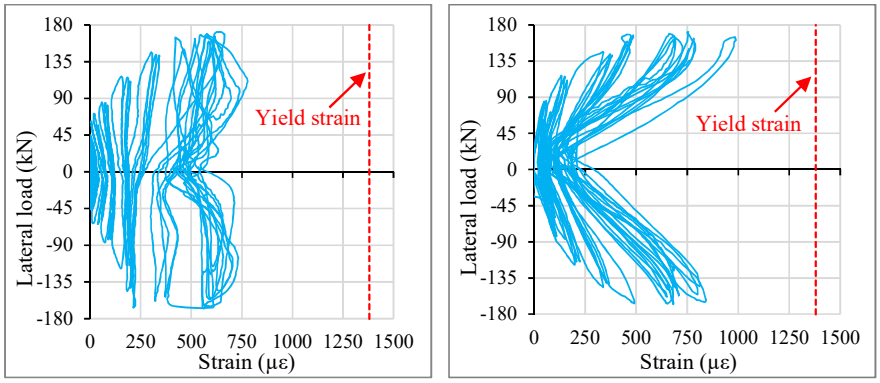

(a) (b)

Figure 11 Lateral load versus strain of the steel tube at gauge point 1: (a) CFST-6SC and (b) CFST-6RB.

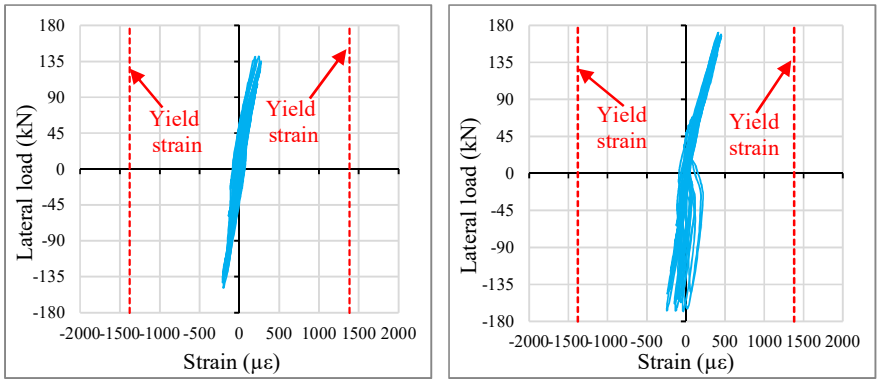

(a) (b)

Figure 12 Lateral load versus strain of the steel tube at gauge point 2: (a) CFST-6SC and (b) CFST-6RB.

3.3 Acceptance Criteria (ACI 374.1-05)

The experimental results were compared with the ACI 374.1-05 criteria [7] to evaluate whether the proposed connections could be used in areas with high seismic risk. The criteria that must be satisfied in such areas are: strength, energy dissipation, and stiffness. ACI 374.1-05 specifies that the specimens must have a lateral strength no less than 75% of the ultimate lateral strength. This should be checked at a drift ratio no less than 3.5%. Table 3 shows that the specimens satisfy the strength criteria of ACI 374.1-05.

Table 3 Strength criteria checking.

Specimen	Direction	Peak lateral strength (kN)	3.5% (third cycle)		4.5% (third cycle)	
			Lateral strength (kN)	Strength ratio > 0.75	Lateral strength (kN)	Strength ratio > 0.75
CFST-6SC	Positive	149.10	137.00	0.92	123.30	0.83
	Negative	141.38	133.30	0.94	107.20	0.76
CFST-6RB	Positive	171.47	150.37	0.88	139.63	0.81
	Negative	167.95	146.24	0.87	138.05	0.82

To check whether the specimens would have sufficient damping after an earthquake, the relative energy dissipation should be higher than 0.125 at a drift ratio of 3.5% (3^{rd} cycle) to meet the ACI 374.1-05 criteria. Table 4 presents the energy dissipation criteria and shows that the specimens satisfied the limits of ACI 374.1-05. In addition, this result also suggests that the minor pinching due to sliding shear has little effect on the overall seismic behavior.

Table 4 Relative energy dissipation checking.

Specimen	Drift ratio	Relative energy dissipation	Remarks
CFST-6SC	3.5 %	0.33	Ok
	4.5 %	0.26	Ok
CFST-6RB	3.5 %	0.35	Ok
	4.5 %	0.28	Ok

During an earthquake, a small lateral load can cause large displacement in building structures, resulting in severe damage. According to ACI 374.1-05, the secant stiffness at a drift ratio of +3.5% to -3.5% should be more than 0.05 of the initial stiffness. This study also found that the performance of the specimens at a drift of 4.5% was good. Table 5 shows that the specimens satisfied the secant stiffness criteria.

Table 5 Secant stiffness checking.

Specimen	Direction	Drift ratio at third cycle	Secant stiffness (kN/mm)	Initial stiffness (kN/mm)	Ratio	Remarks
CFST-6SC	Positive	3.5%	1.86	6.15	0.302	Ok
	Negative		1.80	5.61	0.321	Ok
	Positive	4.5%	1.28	6.15	0.208	Ok
	Negative		1.13	5.61	0.201	Ok
CFST-6RB	Positive	3.5%	2.06	5.17	0.398	Ok
	Negative		2.04	5.03	0.405	Ok
	Positive	4.5%	1.53	5.17	0.296	Ok
	Negative		1.49	5.03	0.296	Ok

4 Finite-Element Analysis

4.1 General

This study developed three-dimensional numerical finite-element models to further comprehend the connections using ANSYS version 19.0 [13]. Several studies [14,15] have shown that ANSYS can accurately model the cyclic behavior of structural elements. Figure 13 shows the finite-element meshes of the specimens. The specimens were modeled as follows: eight-node 3D brick elements (solid 65) were used to model the concrete; two-node 3D spar elements (Link 180) were used to simulate the longitudinal and transversal reinforcements of the beam; 3D solid elements with eight nodes (solid 185) were used to model the steel tube column, shear connector, and supports. Further, contact pairs were implemented to model the interaction of the column with the RC beam and the slip between the beam and the shear connector.

The contact pairs consisted of two elements, namely a target element (TARGE170) and a contact element (CONTA173) with debonding capabilities and the ability to model the surface-to-surface contact between 3D solid elements. The friction coefficient for the contact pairs equaled 0.4. A perfect bond was assigned to the interface between the steel tube and concrete of the column. The FE models ignored the slip between the longitudinal reinforcement bars and the concrete beam.

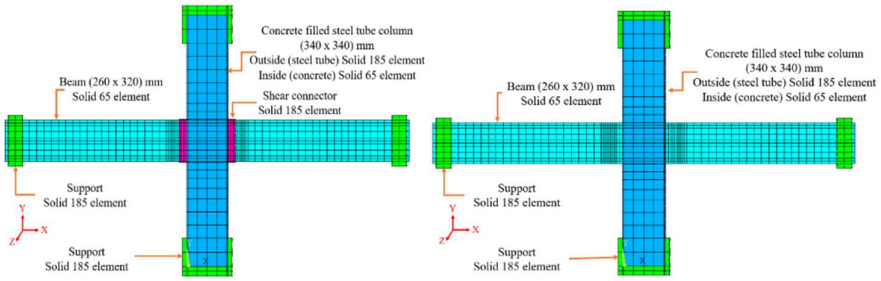

(a) (b)

Figure 13 Finite-element mesh for the specimens (a) CFST-6SC and (b) CFST-6RB.

A multilinear isotropic hardening model in line with Willam and Warnke [16] was used to model the concrete. The shear coefficient for open and close cracks was set to 0.4 and 0.9, respectively. The stress-strain values for the concrete model were obtained from a compression test using an extensometer and were modified by the Hognestad equation as in Figure 14. The modulus of elasticity

(E_c) was obtained from the first point on the stress-strain curve, whereas Poisson's ratio (ν) was assumed to be 0.2. A von Mises yield criterion with bilinear kinematic hardening was used to simulate the elastic and inelastic behavior of the steel components, i.e. the steel plate of the columns, shear connector, and reinforcement bars. Poisson's ratio of 0.3 was used for the steel material. The properties of the steel material used in the FE models were obtained from a tensile test, as shown in Table 1.

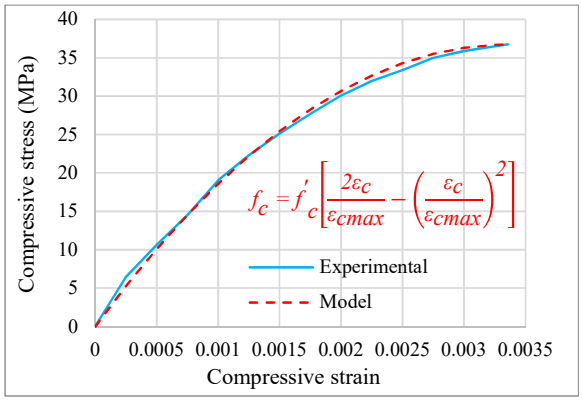

Figure 14 Comparison of the uniaxial stress-strain curve of concrete.

The loading and constraints assigned in the FE models were the same as in the experiments. Two-step loading was used in the FE models. First, an axial load was applied to the column top, followed by cyclic loads. The displacements in the *z* direction at the column top were fully restrained while displacements in the column bottom in each direction were fully restrained to represent pin support. Furthermore, the displacements in the *y* and *z* directions were fully restrained at the end of the beams to represent roller support. The lateral cyclic loading in the FE models was performed only in one cycle at each drift ratio to simplify the analysis.

4.2 Verification of Finite-Element Modeling

To verify the feasibility of the developed FE models, the experimental hysteresis curves of two connection specimens were compared with the FE results, as shown in Figures 15. The comparison of the hysteresis curves showed generally good agreement in terms of strength and deformation, while the loading and unloading stiffness in the FE models was less obvious than in the experimental curves.

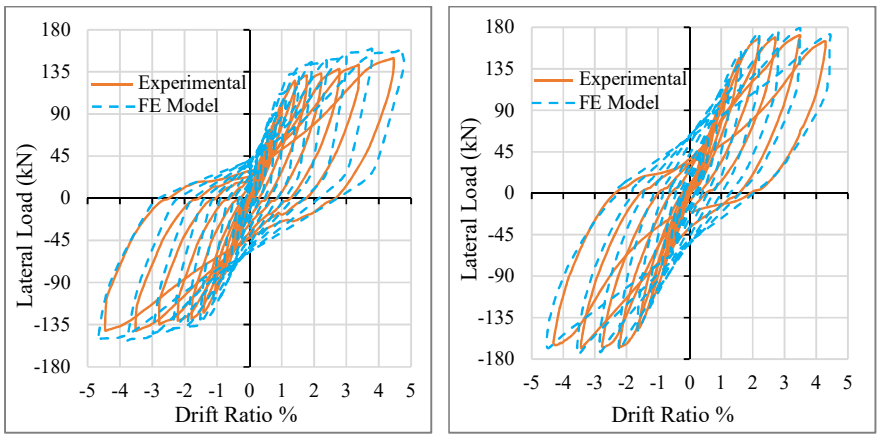

(a) (b)

Figure 15 Comparison of hysteresis curves for (a) CFST-6SC, and (b) CFST-6RB.

Table 6 shows a comparison of yield and ultimate lateral strength between the experimental and the FE results. This comparison showed that the results of the FE model closely resembled the experimental ones. The difference between the FE models and experimental results can be attributed to: (i) mesh refinement, (ii) idealized boundary conditions in the FE models, and (ii) material nonlinearity (material properties/models available in ANSYS).

Table 6 Comparison of experimental and FE results under cyclic loading.

Specimen	Loading direction	Yield lateral strength (kN)			Ultimate lateral strength (kN)		
		P_{ye}	P_{yFEM}	P_{yFEM}/P_{ye}	P_{ue}	P_{uFEM}	P_{uFEM}/P_{ue}
SCFST-6SC	Positive	105.3	110.9	1.05	149.1	158.9	1.07
	Negative	104.2	106.5	1.02	141.4	151.3	1.07
SCFST-6RB	Positive	129.8	133.5	1.03	171.4	178.1	1.05
	Negative	128.5	132.7	1.03	167.9	175.3	1.04

Note: P_{ye} and P_{yFEM} are the yield and ultimate strengths from the experimental and finite element results, respectively.

4.3 Principal Stress Distribution

Figures 16 and 17 show the principal stress distribution in the specimens at peak lateral strength. These figures show that an obvious diagonal strut action was formed in the joint zone by normal concrete and steel stresses at the boundary of the connection. In both specimens, diagonal strut action occurred at the joint zone at drift ratio 0.5%. The diagonal strut widened because the stress continued to increase according to the loading history. The diagonal strut of the CFST-6RB

specimen was larger than in the CFST-6SC specimen because of the additional web reinforcement which increased the forces acting on the joint.

The stress in the steel tube of both specimens remained below the yield strength. This corresponds to Figures 11 and 12. The concrete of the joint was in a state of triaxial stress and the principle stress remained below the average compressive strength. This corresponds to absence of cracks in the joint zones in both test specimens (see Figure 9(a-b)). This enhancement can be explained by the confinement provided by the outer steel tube.

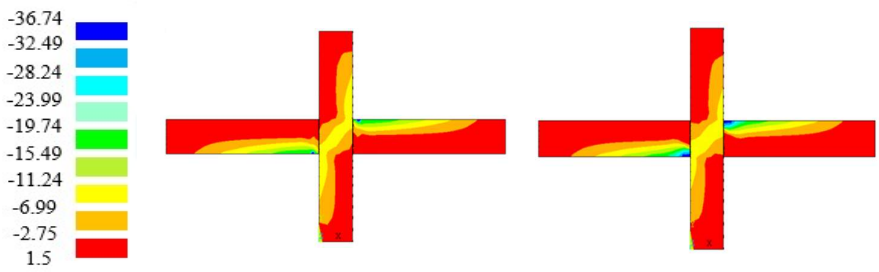

Figure 16 Principal stress distribution in MPa for the concrete in the column and the beam: (a) CFST-6SC, and (b) CFST-6RB.

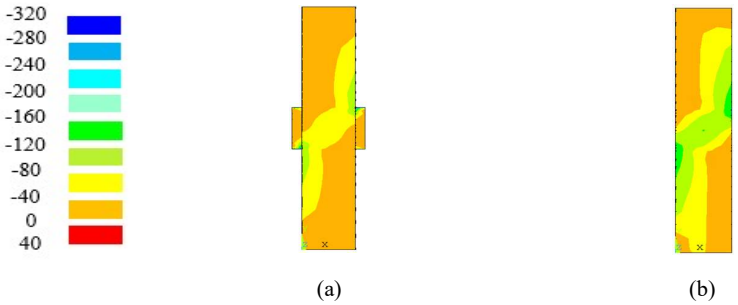

Figure 17 Principal stress distribution in MPa for the steel tube column: (a) CFST-6SC, and (b) CFST-6RB.

5 Conclusion and Recommendations

The seismic behavior of novel connections was investigated experimentally and numerically. The conclusions are summarized below.

This research evaluated a new connection system to connect CFST columns and RC beams that provides joint confinement through a continuous steel tube. The columns of the specimens were designed according to the AISC 360 criteria [11], while the beam-design was based on the ACI 318 criteria [10]. The joint shear strength was calculated according to the AIJ standard [12]. Sliding shear in the design was expected because of the smooth continuous steel tube at the beam-to-column interface. Two specimens were designed and fabricated, which differed in how they prevented the sliding shear mechanism. Potential sliding shear can be better mitigated if sufficient continuous longitudinal web reinforcement is provided at the beam. Although minor sliding shear was observed during the test, it did not affect the overall seismic behavior set by ACI374.1-05 [7]. The specimens achieved the desired seismic design objective of a strong column (strong joint)/weak beam. The test results showed that continuous steel tubes provide sufficient joint confinement to prevent the occurrence of cracks and to control shear deformation of the joint. In addition, the new connections possess good stiffness, strength, and energy dissipation capacity.

The study also developed FE models to further investigate the performance of the new connections under cyclic loading. To ensure the validity of the models, the study validated and verified the experimental data. The cyclic response from the FE models correlated well with the experimental results. In addition, the principal stress analysis showed that a concrete and steel diagonal strut is formed in the joint.

It can be concluded that the novel connections have excellent seismic performance and can potentially be used in building construction in precast systems. The proposed system to connect the CFST column to the RC beam is an effective precast connection that has good performance during earthquakes and can be applied in zones with strong earthquakes. Construction efficiency can be obtained by reducing formwork and reinforcing bars. In addition, the casting of concrete through a pump-up method can lead to the reduction of manpower, construction costs, and time. Lastly, the proposed connection types are easy to construct and architecturally desirable.

Acknowledgements

Financial support for this study was provided through the Research, Community Service and Innovation Program (P3MI) and the Faculty of Civil and Environment Engineering, Institut Teknologi Bandung, Indonesia.

References

[1] Gourley, B.C., Tort, C.T., Denavit, M.D., Schiller, P.H. & Hajjar, J.F., *A Synopsis of Studies of the Monotonic and Cyclic Behavior of Concrete-Filled Steel Tube Members, Connections, and Frames*, Technical Report, Department of Civil and Environmental Engineering, University of Illinois at Urbana-Champaign, 2008.

[2] Chen, Q.J., Cai, J., Bradford, M.A., Liu, X. & Zuo, Z.L., *Seismic Behaviour of a Through-Beam Connection between Concrete-Filled Steel Tubular Columns and Reinforced Concrete Beams,* Engineering Structures, **80**, pp. 24-39, 2014.

[3] Chen, Q.J., Cai, J., Bradford, M.A., ASCE, D.M., Liu, X. & Wu, Y., *Axial Compressive Behavior of Through-Beam Connections between Concrete-Filled Steel Tubular Columns and Reinforced Concrete Beams*, Journal of Structural Engineering, **141**(10), pp. 1-13, 2015.

[4] Tang, X.L., Cai, J., Chen, Q.J., Liu, X. & He, A., *Seismic Behaviour of Through-Beam Connection between Square CFST Columns and RC Beams*, Journal of Constructional Steel Research, **122**, pp. 151-161, 2016.

[5] Zhang, Y.F., Zhao, J.H. & Cai, C.S., *Seismic Behavior of Ring Beam Joints between Concrete-Filled Twin Steel Tubes Columns and Reinforced Concrete Beams*, Engineering Structures, **39**, pp. 1-10, 2012.

[6] Zhou, X., Cheng, G., Liu, J. Gan, D. & Chen, Y.F., *Behavior of Circular Tubed-RC Column to RC Beam Connections under Axial Compression*, Journal of Constructional Steel Research, **130,** pp. 96-108, 2017.

[7] ACI Committee 374.1, *Acceptance Criteria for Moment Frames Based on Structural testing, and Commentary*, ACI 374.1-05, Farmington Hills, United States, 2005.

[8] American Society of Testing Materials (ASTM) International, ASTM C39/C39M-15a. *Standard Test Method for Compressive Strength of Cylindrical Concrete Specimens*, Washington D.C., 2015.

[9] American Society of Testing Materials (ASTM) International, ASTM A370, *Standard Test Methods for Tension Testing of Metallic Materials*, Washington D.C., 2015.

[10] ACI Committee 318, *Building Code Requirements for Structural Concrete and Commentary (ACI 318-19),* ACI, Farmington Hills, United States, 2019.

[11] AISC Committee, *AISC Specification for Structural Steel Buildings (ANSI/AISC 360-16)*, American Institute of Steel Construction, USA,2016.

[12] Architectural Institute of Japan (AIJ), *Standard for Structural Calculation of Steel Reinforced Concrete Structures*, 5th Ed, AIJ, Tokyo, Japan, 2001.

[13] ANSYS v.19.1, program manual, 2019.

[14] Budiono, B., Dewi, N.T.H. & Lim, E., *Finite Element Analysis of Reinforced Concrete Coupling Beams*, Journal of Engineering and Technological Sciences. **51**(6), pp. 762-771, 2019.
[15] Budiono, B., Nurjannah, S.A. & Imran, I., *Non-linear Numerical Modeling of Partially Pre-stressed Beam-column Sub-assemblages Made of Reactive Powder Concrete*, Journal of Engineering and Technological Sciences. **51**(1), pp. 28-47, 2019.
[16] William K.J., and Warnke E.P., *Constitutive Model for the Triaxial Behavior of Concrete*, Proceedings of the International Association for Bridge and Structural Engineering, ISMES, Bergamo, Italy, **19**, 1975.